UNIABUJA Journal of Engineering and Technology

https://ujet.uniabuja.edu.ng/

ISSN: 2714-3236 (Online); 2714-3228 (Print)

Volume 3, Issue 1, 2025; 98-110

Fault Identification and Location System for 11 kV Distribution Line Using Magneto-Resistive Sensing

Advocate I. TOMMY[1], Muhammad UTHMAN[2], Ozovehe S. ALIYU[3]

[1,2,3]Department of Electrical/Electronic Engineering, University of Abuja, Abuja, Nigeria

[1]advocatetommy57@gmail.com, [2] m.uthman@yahoo.com, [3]aliyu123oz@gmail.com

Abstract

Timely fault detection and location are of paramount importance in ensuring the reliability of the power distribution system. While there are many methodologies for detecting and locating faults, timely, accurate, and inexpensive fault location is necessary. This paper explores the use of magneto-resistive sensing to develop a system for fault detection and location on an 11kV distribution line as an improvement over systems that are already being used. To achieve this, fault data and load profile were collected from Dutse Alhaji Injection Substation and used to model a system with different fault scenarios, using Convolutional Neural Network (CNN). The modelled base case network was accurate and corresponded to the theoretical result. Eighty percent of the data was used to train the system, and twenty percent was reserved for testing. A feedback loop was implemented in real-time performance, incorporating operator feedback. The magnetic field at fault was transduced to an electrical quantity. The proposed system was able to detect fault location using the corresponding electromagnetic field, which varied inversely with the distance of the fault. Results were analysed and validated. The error was 4.98%.

Keywords: *Magnetoresistive sensing, fault impedance, single-line-to-ground fault, double line fault, double line to ground fault, three phase fault.*

1.0 Introduction

The reliability and efficiency of electrical power systems are critical to the stability of industrial operations and residential energy use. The distribution system is an indispensable component of the power systems. In Nigeria, it is common knowledge that power generation is abysmally low in comparison to the demand. As a result, load shedding has become a usual daily routine for power systems operators. Extended outages due to faults further exacerbate the situation.

In Nigeria, distribution voltage levels are 11 kV on the High Tension (HT) line and 400 V on the Low Tension (LT) line. This is stepped down from higher voltages to ensure the safety of end-users and their equipment. The need to ensure minimal downtime, rapid fault resolution, and improved system resilience is paramount. Among the various components of the power delivery chain, the 11 kV feeders form a vital link between substations and the end-users. However, these lines are prone to various short circuit faults, which may result in outages, equipment damage, and sometimes safety hazards. These faults may be caused by insulation failure, lightning, trees falling across lines, birds shorting lines, line breaks due to excessive loading, vehicles colliding with poles, equipment failure, flashovers that cause insulators to lose insulating capability due to high voltage, smoke from fires, aging and weakness of equipment and cables, human errors, intentional damage, and so on (Baladuraikannan, 2023). Consequently, the precise and timely identification and repair of faults in distribution cables have become an especially pressing concern (Widodo et al., 2021; Ngwenyama et al., 2021). Power distribution faults represent the most prevalent disturbances encountered in voltage distribution networks (Jeevan, 2022). They pose a dual risk to equipment and individuals while diminishing the quality and reliability of electricity distribution. The pivotal challenge for network operators lies in the detection and precise localization of these earth faults.

Consequently, there exists a continual need to refine criteria that facilitate an unambiguous evaluation of the current state of the network (Stefanidou-Voziki et al., 2022). This article is dedicated to assessing the effectiveness of the traditional zero-sequence overcurrent criterion and investigating modifications to the zero-sequence overcurrent criterion employed in fault current passage indicators, which are instruments designed to efficiently identify and pinpoint earth faults. In this context, two novel adaptation criteria tailored for networks with resistor-grounded neutral points have been put forth (Majidi et al., 2014). These criteria substantially enhance the efficiency of earth fault detection, especially for high-impedance cases. Computational and simulation-based verification demonstrates that in specific scenarios, these proposed

Received: 11-07-2026 / Accepted: 12-12-2025 / Published: 29-01-2026

https://doi.org/10.70118/ujet.2026.0301.10

solutions can outperform the classic criterion by over 40%. Moreover, they significantly augment the value of the detected transition resistance RF (Ogomaka et al., 2020). The aforementioned advantages collectively underscore the potential practical benefits of adopting these criteria (Bakar et al., 2014).

The absence of a securely earthed natural point leads to a reduced magnitude of phase-to-earth fault current (Orlowski, 2006). In such a case, the short-circuit current usually remains close to the load current's value. Consequently, maintaining the effective performance of phase-to-earth fault protection relays becomes more challenging, as noted in reference (Majidi & Etezadi-Amoli, 2017). Many times, the measured quantities' amplitudes are akin to the background noise levels, which becomes a noteworthy concern, especially in networks employing Petersen coils to ground the neutral point (Silos-Sanchez, 2020). To aid this research work, a comprehensive review of past and present similar works was carried out to create a relationship between this research work and studies that had already been done. This was with a view to serving as a guide towards achieving the set aim and objectives of this research work.

1.1 Time Domain Reflectometry

Time Domain Reflectometry (TDR) uses a pulse echo range-finding technique to measure the distance to changes in the cable structure. By these methods, short-duration low-voltage pulses (up to 50 V) are transmitted at a high repetition rate into the cable, and the time taken for them to reflect from areas where the cable has low impedance, such as at a fault, is measured. The reflections are traced on a graphical display with amplitude on the y-axis and elapsed time, which is directly related to the distance to the position of the fault, on the x-axis. The TDR does not cause insulation degradation because a low-energy signal is sent through the cable. A theoretically perfect cable returns the signal in a known time and in a known profile. One weakness of TDR is that it does not exactly pinpoint the faults. Its accuracy is within about 5% of the testing range. Sometimes, this information alone is sufficient. Another weakness of TDR is that reflectometers cannot only detect faults with resistances much greater than 200 ohms. Where there is a bleeding fault, or rather than a short or near-short, TDR cannot detect the fault (Rao, 2020; Loete, 2023).

1.2 Acoustic Fault Location Method

This method is used for pinpointing faults of high resistance and intermittent faults in buried cable when the cable is subjected to a series of high voltage pulses, which are sent down the cable, causing the fault to break down. This is called thumping. During a flashover, an audible acoustic signal is generated that can be detected on the ground surface using a ground microphone, receiver, or headphone. The amplitude of the flashover sound gets higher when the distance to the fault is closer (Albert, 2022). This method is usually not done on live cables, so it is difficult to detect a fault in real time. It also requires huge cost, time, and human effort in finding the location of the fault.

1.3 Distributed Temperature Sensing (DTS)

DTS equipment is always installed for new cable systems so as to identify faulty cross-bonding and to enable dynamic line rating. The optical fibre should be close to or embedded in the faulty core. Traditionally, a fault is detected by thumbing the cable repeatedly with high voltage pulses. This makes the fault location hotter than the rest of the cable. With this method, the fault on the two other phases would not be found by monitoring just one cable length (Albert, 2022; Mohamed, 2021). Apart from the first current sensing method as given in 1.1, the other techniques above face the following challenges:

i) All are offline methods in that they are used to detect fault location after it has occurred, and the cables have been de-energized, while the proposed system is an online technique.

ii) The overall cost of the locator unit can be much higher than the proposed system.

iii) Result interpretation can be very tricky.

iv) The process of fault location can be very tedious in more complex power systems

compared to single-line cables.

v) As mentioned earlier in 1.1, there is a need to install many sensors at different locations to detect and analyse fault current. For three lines, there is a need to have up to three sensors at each location. The cost implication of this will be huge (Mohamed, 2021)

In consideration of the techniques mentioned above, magnetoresistive sensing was proposed for faults and location in real time, with minimal cost and safety to personnel.

2.0 Methodology

2.1 Magneto-resistive Sensing

Received: 11-07-2026 / Accepted: 12-12-2025 / Published: 29-01-2026

https://doi.org/10.70118/ujet.2026.0301.10

The principle of this research is based on the magnetic field of the overhead line conductors. In an electric field, there is an associated magnetic field. A current in an electric field produces a magnetic field that has direct proportionality to the electric current (Shneidman, 2025). In magnetoresistive sensing faults are measured by converting the corresponding magnetic field under fault conditions. This concept is illustrated in Biot-Savart Law, which is expressed as:

2.2 Magnetic Field from Line Current

According to Biot–Savart Law, a line current I, produces a magnetic field B around the conductor:

$$\mathbf{B} = \frac{\mu_0}{4\pi} \int \frac{I\, d\mathbf{l} \times \hat{\mathbf{r}}}{r^2} \quad (1)$$

For a long straight conductor:

$$B(r) = \frac{\mu_0 I}{2\pi r} \quad (2)$$

where:

- $B$is magnetic flux density (Tesla)
- $I$is current (A)
- $r$is distance from conductor (m)
- $\mu_0$is permeability of free space ($\approx 4\pi \times 10^{-7}$) (Shneidman, 2025)

It can be seen that under normal conditions, the electromagnetic field will be seen as shown below:

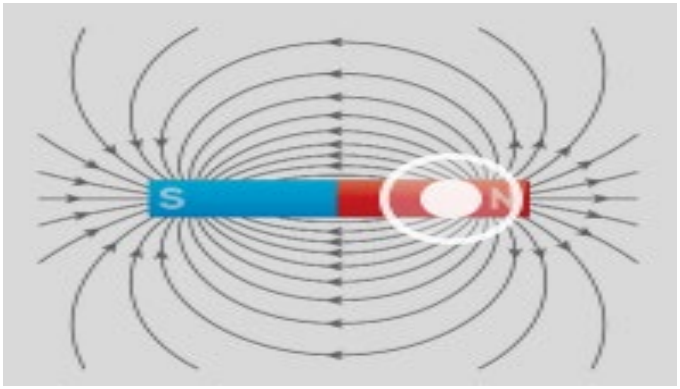

Figure 1: Electromagnetic field under normal conditions (Shneidman, 2025)

It can be seen that though the current is confined within a conductor, the corresponding electromagnetic field spreads around it. If an electromagnetic sensor is placed within the electric field, it responds proportionately to the magnetic field of the electric current. During faults, the fault current increases beyond what is normal. There is also a corresponding increase in the electromagnetic field beyond the normal threshold value. When faults occur, the magneto-resistive sensor detects the corresponding magnitude of magnetic field, the resistance of which varies with the applied magnetic field. Being a transducer, it replicates an equivalent electrical quantity, which is fed into an Arduino for communication with an external mobile device (Rao, 2020).

There are several kinds of magneto-resistive sensors. Giant Magneto Resistive (GMR), was preferred because of its capabilities. It is more accurate and reliable than other types of touch screen sensors. Its sensitivity can detect as little as the Earth's magnetic field (Pratiwi, 2020). In order to mitigate the effects caused by Earth's MF and noise in electronic devices, the TMR sensor is connected through a high-pass filter, and then the output signal is amplified by a low-noise instrumentation amplifier (AD8421, 3nV/ √Hz). The amplified signal is then sampled at a sampling frequency of 5 kHz using 16 16-bit, six-channel Analog-to-Digital Converter (Fernandez, 2024; Kazim et al., 2024).

2.3 Conductor Configuration

The conductors of the overhead lines are arranged in any of these three configurations: vertical, horizontal, and triangular.

Received: 11-07-2026 / Accepted: 12-12-2025 / Published: 29-01-2026
https://doi.org/10.70118/ujet.2026.0301.10

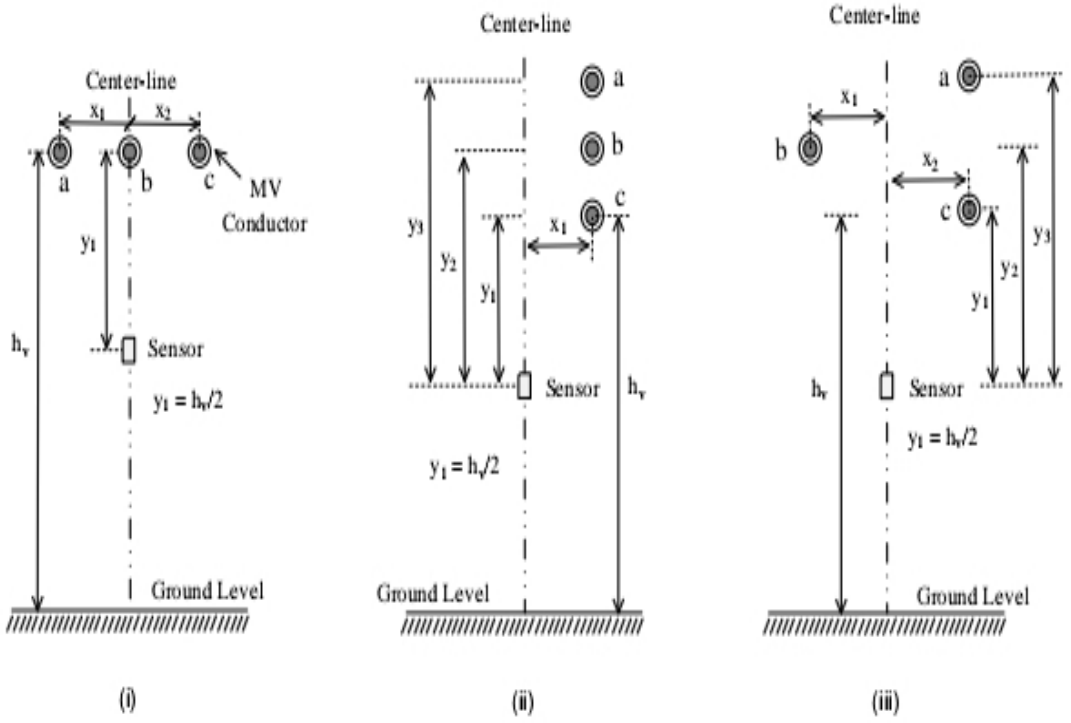

Figure 2: Geometric representation of 11kV overhead conductor's configuration and sensor installation (Wang, 2023)

The simulation was done based on vertical configuration.

2.4 Model Development Radial Network of Dutse Alhaji Injection Substation

The fault detection and classification simulation was designed using four different methods: Single Line to Ground (SLG), Double Line (DL), Double Line to Ground (DLG), and Three Line (TL). Development was carried out in Python, with a high-level API Convolutional Neural Network for fault detection for Tensor BFS power flow that facilitates model building and training. CNN allows models to be constructed by arranging layers in specific configurations, such as Sequential or Functional. For this project, a Sequential configuration, a linear stack of layers was chosen as it is well-suited for deep learning (Wang, 2023; Dehkordi, 2020).

2.4.1 Line Data

The resistance of the distribution line was measured in Ohms. The capacitive effect of the distribution line, though negligible, was included for completeness. It is measured in Ohms. The combined resistance and reactance of the line was used as a complex number. An allowable voltage range of 10.8kV and 11.2kV was considered for the simulation. The line data used were obtained from the Transmission Company of Nigeria (TCN).

2.4.2 Load Data

Active Power Demand: The active power consumed at the buses (in MW) of the network, taken over a period of six months, was used.

Reactive Power: Reactive power (in KVAR) generated at the buses was considered. These data were obtained from the Abuja Electricity Distribution Company (AEDC).

2.5 Mathematical Modelling

The magnitude of fault currents for different fault scenarios can be calculated using the formulae as outlined below:

2.5.1 Single Line to Ground Fault (SLGF):

$$\boldsymbol{If = 3V/(Z1 + Z2 + Z0 + Ze + 3Zf)} \quad (3)$$

Where I_f = is fault current, Z1, Z2, and Z0 are positive sequence, negative sequence, and zero sequence impedances, respectively, while Ze and Zf are earth impedance and fault impedance, respectively (Emechebe, 2021).

If Ze and Zf are zero, Eqn 3 is simplified to:

$$If = 3V/(Z1 + Z2 + Z0) \quad (4)$$

Received: 11-07-2026 / Accepted: 12-12-2025 / Published: 29-01-2026

https://doi.org/10.70118/ujet.2026.0301.10

2.5.2 Double Line Fault (DLF)

A double-line fault can occur with or without fault impedance. The following expressions are obtainable in calculating Double Line Fault current:

$$If = -j1.732V/(Z1 + Z2) \quad (5)$$

Where V is the voltage, Z1 and Z2 are positive and negative sequence impedances, respectively, and the fault impedance is zero (Baladuraikannan, 2023).

For a double line fault where fault impedance is present, the fault current is given as:

$$If = -j1.732V/(Z1 + Z2 + Zf) \quad (6)$$

Where V is the voltage, Z1 and Z2 are positive and negative sequence impedances, respectively [1].

2.5.3 Double Line to Ground Fault (DLGF)

For DLGF without fault impedance, the fault current is given as:

$$If = -3VZ2/Z1(Z0 + Z2 + Z0Z2) \quad (7)$$

Where V is the voltage, Z1, Z2, and Z0 are the positive, negative, and zero sequence impedances, respectively (Baladuraikannan, 2023).

If fault impedance exists, fault current is expressed as:

$$If = -3(V - IR1 - Z1)/(Z0 + 3Zf) \quad (8)$$

Where Z1, Z0, and Zf are positive, negative, and fault impedances, respectively, and I_{R1} is the current on Phase A (Baladuraikannan, 2023).

2.5.4 Three-Phase Fault (TPF)

For a three-phase fault, the fault current is expressed as:

$$If = V/Z1 \quad (9)$$

Where Z1 is the positive sequence impedance (Emechebe, 2021).

2.5.5 Three-Phase to Ground Fault (TPGF)

For three three-phase to ground fault, the fault current is given by:

$$If = V/(Z1 + Zf) \quad (10)$$

Where Z1 is the positive sequence impedance (Emechebe, 2021).

2.5.6 Normal Phase Currents

Phase currents under normal conditions are given as follows:

$$IR = PaSin(\omega t)/(1.732V) \quad (11)$$

$$IY = PaSin(\omega t - 120)/(1.732V) \quad (12)$$

$$IB = PaSin(\omega t + 120)/(1.732V) \quad (13)$$

Where P_a is the peak apparent power of the substation, I_R, I_Y, and I_B are currents on Phase A, Phase B, and Phase C, respectively (Emechebe, 2021).

2.6 CNN MODEL

2.6.1 CNN Flowchart

The flowchart for this research is as shown in Figure 3.

Received: 11-07-2026 / Accepted: 12-12-2025 / Published: 29-01-2026
https://doi.org/10.70118/ujet.2026.0301.10

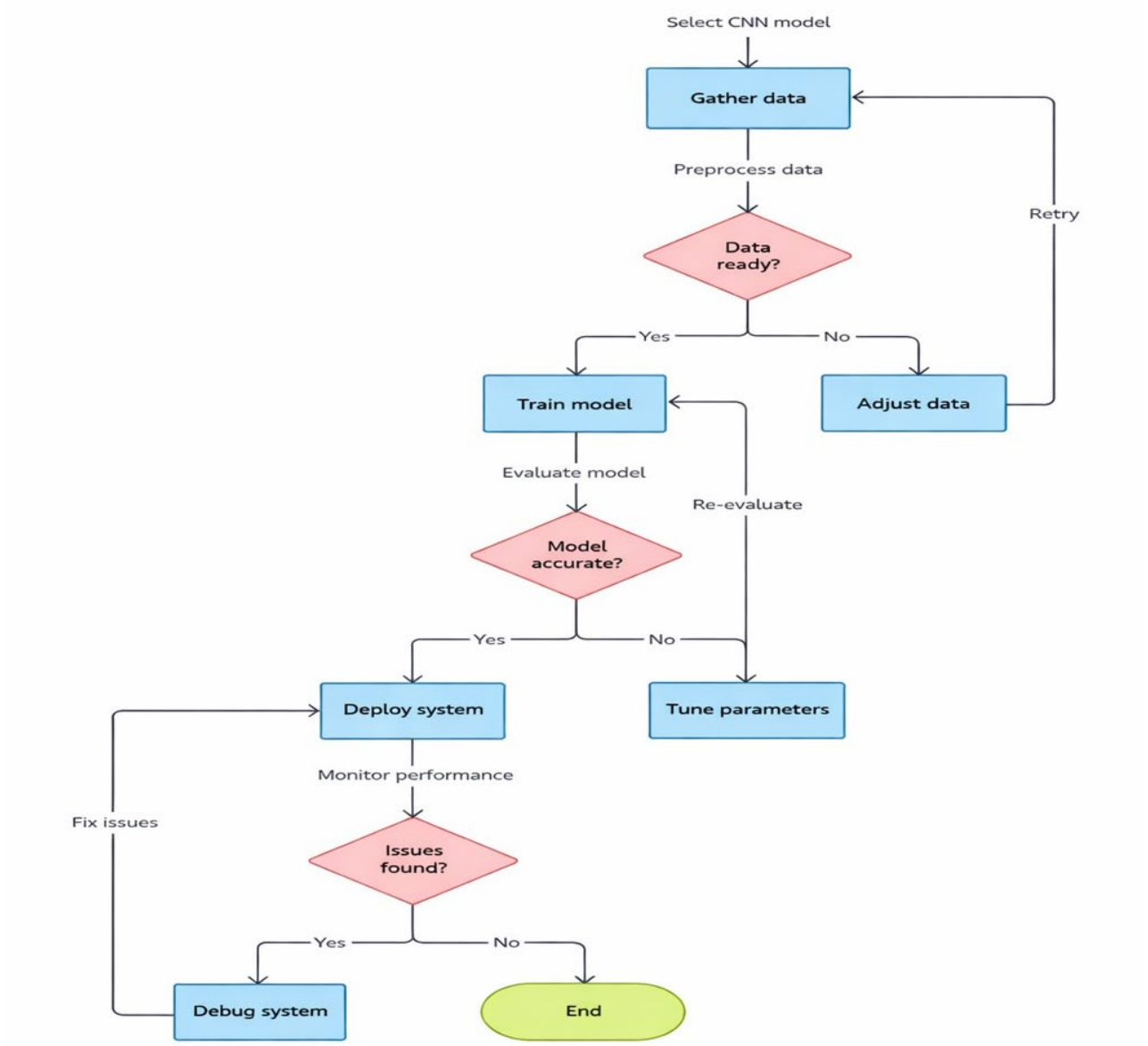

Figure 3: CNN flowchart (Lecun et al., 2015)

2.7 CNN Algorithm

An existing deep learning CNN algorithm was used in the implementation of this work. 80% of the dataset was used for training the model, while 20% was for testing. The data size was 2500, collected for a period of five years (2018-2023).

3.0 Results and Discussions

Three scenarios were considered and modelled using Convolutional Neural Network Model configuration for fault detection and location. The proposed method was implemented on Dutse Alhaji Injection Substation distribution network. Backward-Forward Sweep was used for the power flow analysis, CNN optimal fault detection and location, and opening of tie-line and sectionalizing switches.

3.1 Normal Loading Condition

The waveform of current under normal loading condition was obtained as shown below:

Received: 11-07-2026 / Accepted: 12-12-2025 / Published: 29-01-2026
https://doi.org/10.70118/ujet.2026.0301.10

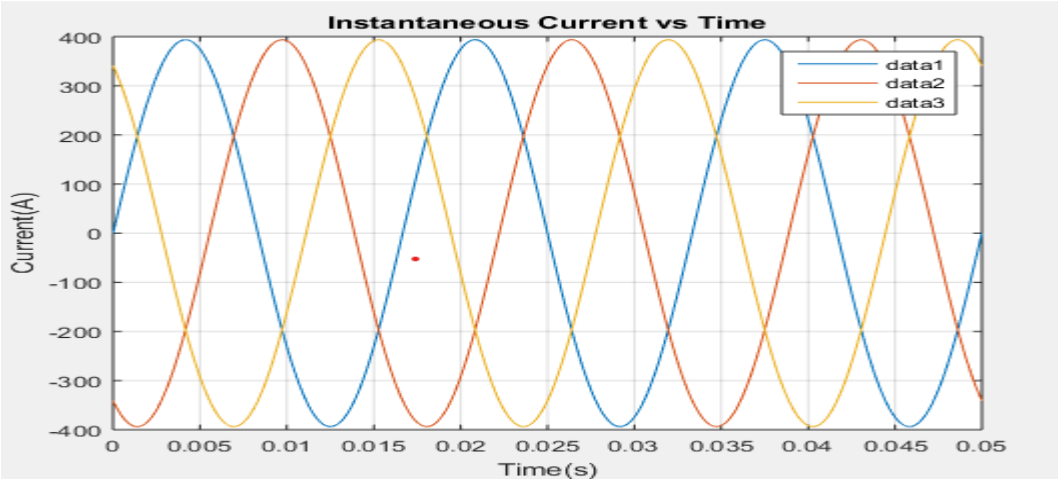

Figure 4: A plot of current vs time under normal conditions

The RMS value of current obtained was 393.66A. The blue, red and yellow graphs represent the three different phases which were 120° apart. This was the normal system current. The system did not show any response to fault. The system did not respond to an overload of less than 10%. A threshold valued of 433A was allowed beyond which the system detected fault occurrence.

The instantaneous current of phase $\boldsymbol{k}(\boldsymbol{k} \in \{\boldsymbol{a}, \boldsymbol{b}, \boldsymbol{c}\})$ be expressed as:

$$\boldsymbol{i_k(t) = I_{m,k} \sin(\omega t + \phi_k)} \quad (14)$$

where:

$\boldsymbol{I_{m,k}}$ is the peak current magnitude of phase $\boldsymbol{k}$,

$\boldsymbol{\omega = 2\pi f}$ is the angular frequency,

$\boldsymbol{\phi_k}$ is the phase angle.

The root mean square (RMS) value of the phase current over one fundamental cycle $\boldsymbol{T}$ is given by:

$$\boldsymbol{I_{k,\mathrm{RMS}} = \sqrt{\frac{1}{T}\int_0^T i_k^2(t)\, dt}} \quad (15)$$

For a pure sinusoidal waveform, this simplifies to:

$$\boldsymbol{I_{k,\mathrm{RMS}} = \frac{I_{m,k}}{\sqrt{2}}} \quad (16)$$

In discrete-time implementation, suitable for digital signal processing and CNN input preparation, the RMS current is computed as:

$$\boldsymbol{I_{k,\mathrm{RMS}} = \sqrt{\frac{1}{N}\sum_{n=1}^{N} i_k^2(n)}} \quad (17)$$

where $\boldsymbol{N}$ is the number of samples per cycle (Shrawane & Sidhu 2021; Alqusayer & Habibaballah, 2022).

System Rated Current and Overload Margin:

Let the rated RMS current of the distribution line be denoted as:

$$\boldsymbol{I}_{\mathrm{rated}}$$

The system allows a permissible overload margin of 10%, reflecting normal operational variations and short-term load surges. The overload threshold is therefore defined as:

$$\boldsymbol{I}_{\mathrm{OL}} = \boldsymbol{1.1 \times I}_{\mathrm{rated}} \quad (18)$$

Any current magnitude satisfying:

$$\boldsymbol{I_{k,\mathrm{RMS}} \leq I}_{\mathrm{OL}}$$

is classified as normal or overload operation, and must not trigger fault detection.

Fault Detection Thresholding Logic:

The fault detection criterion was formulated as:(Shrawane & Sidhu, 2021)

$$\text{Fault Condition} = \begin{cases} \boldsymbol{0}, & \boldsymbol{I_{k,\mathrm{RMS}} \leq 1.1\, I}_{\mathrm{rated}} \\ \boldsymbol{1}, & \boldsymbol{I_{k,\mathrm{RMS}} > 1.1\, I}_{\mathrm{rated}} \ \wedge\ \boldsymbol{\mathcal{F}(i_k(t)) = 1} \end{cases} \quad (19)$$

where:

0 denotes no fault,

1 denotes fault detected,

$\boldsymbol{\mathcal{F}(i_k(t))}$ represents the CNN-based feature classifier that evaluates waveform distortions, asymmetry, and transient signatures.

This dual-condition approach ensures that magnitude alone does not result in false fault classification, particularly during permissible overload conditions.

Application to the Observed Result:

From the measured waveform in Figure 4, the maximum RMS current is:

Received: 11-07-2026 / Accepted: 12-12-2025 / Published: 29-01-2026

https://doi.org/10.70118/ujet.2026.0301.10

$\boldsymbol{I}_{\text{RMS,max}} = \mathbf{393.66}$ A
Given that:
$\boldsymbol{I}_{\text{RMS,max}} \leq \mathbf{1.1}\, \boldsymbol{I}_{\text{rated}}$
and the waveform remains sinusoidal and balanced across all three phases, the fault condition evaluates to:

$$\text{Fault Condition} = \mathbf{0}$$

The results show that the system, when implemented, would detect faults without physical contact with the lines but through a field using magneto-resistive sensors, which act at a distance from the distribution lines. If the maximum allowable current on the distribution line is exceeded, the sensor will be activated for tripping function.

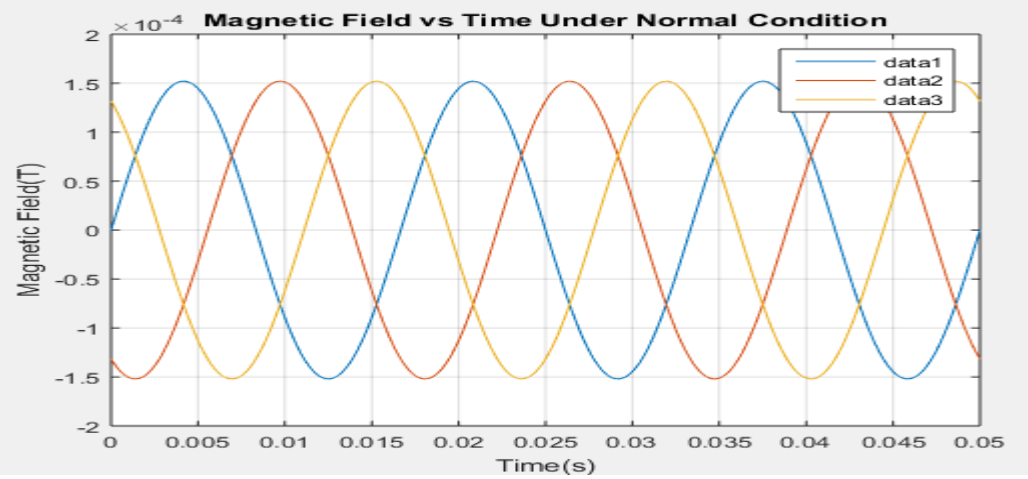

Figure 5: Magnetic field under normal conditions

The magnetic field under normal conditions, with the sensor at a vertical distance of 5.18m gave the result as shown in the graph above. As previously stated, for a straight, long conductor carrying instantaneous current $\boldsymbol{i(t)}$, the magnetic flux density at a radial distance $\boldsymbol{r}$, from the conductor is governed by Ampère's law:

$$\boldsymbol{B(t)} = \frac{\boldsymbol{\mu_0 \mu_r}}{\boldsymbol{2\pi r}}\, \boldsymbol{i(t)}$$

where:
$\boldsymbol{B(t)}$= instantaneous magnetic flux density (T),
$\boldsymbol{\mu_0} = \mathbf{4\pi \times 10^{-7}}$ H/m= permeability of free space,
$\boldsymbol{\mu_r}$= relative permeability of the surrounding medium (≈ 1 for air),
$\boldsymbol{r}$= perpendicular distance between conductor and sensor (m).

Since the magneto-resistive sensor responds to the magnetic field generated by the line current, the RMS magnetic field is derived directly from the RMS current (Shneidman, 2025).

$$\boldsymbol{B}_{\text{RMS}} = \sqrt{\frac{\mathbf{1}}{\boldsymbol{T}} \int_0^T \boldsymbol{B^2}\,(\boldsymbol{t})\, \boldsymbol{dt}} \qquad (20)$$

Substituting $\boldsymbol{B(t)}$from Ampère's law:(Shrawane & Sidhu, 2021)

$$\boldsymbol{B}_{\text{RMS}} = \frac{\boldsymbol{\mu_0 \mu_r}}{\boldsymbol{2\pi r}}\, \boldsymbol{I}_{\text{RMS}} \qquad (21)$$

This equation provides a direct linear mapping between the measured RMS current and the corresponding RMS magnetic field.
Magnetic Field Threshold for Fault Detection:
Given the current-based fault threshold:

$$\boldsymbol{I}_{\text{fault}} = \mathbf{1.1} \times \boldsymbol{I}_{\text{rated}} \qquad (22)$$

the corresponding magnetic field fault threshold is defined as:

$$\boldsymbol{B}_{\text{fault}} = \frac{\boldsymbol{\mu_0 \mu_r}}{\boldsymbol{2\pi r}}\,(\mathbf{1.1} \times \boldsymbol{I}_{\text{rated}}) \qquad (23)$$

Thus, the magnetic field decision rule became: (Alqusayer & Habiballah, 2022)

$$\text{Fault Condition} = \begin{cases} \mathbf{0}, & \boldsymbol{B}_{\text{RMS}} \leq \boldsymbol{B}_{\text{fault}} \\ \mathbf{1}, & \boldsymbol{B}_{\text{RMS}} > \boldsymbol{B}_{\text{fault}} \end{cases} \qquad (24)$$

The maximum magnetic field was 1.5 x 10^ − 4 T. Since the system was normal, the B_{RMS} was returned as 0, indicating that no fault had occurred.

3.2 Single Line-to-Ground Fault (SLGF)

In the Single Line to Ground Fault scenario, the fault current was detected in one phase. The fault current, as detected, was when it was in excess of 15% of the full load value. The sensor would send a tripping signal after this threshold. The system parameters, such as base voltage, line impedance, fault impedance, and fault location, were detected during a fault when the single-phase distribution line is out. It then calculates voltages

Received: 11-07-2026 / Accepted: 12-12-2025 / Published: 29-01-2026
https://doi.org/10.70118/ujet.2026.0301.10

and currents for pre-fault, fault, and post-fault conditions based on a single line-to-ground fault. It plots the voltage and current graphs during the fault scenario at every time interval.

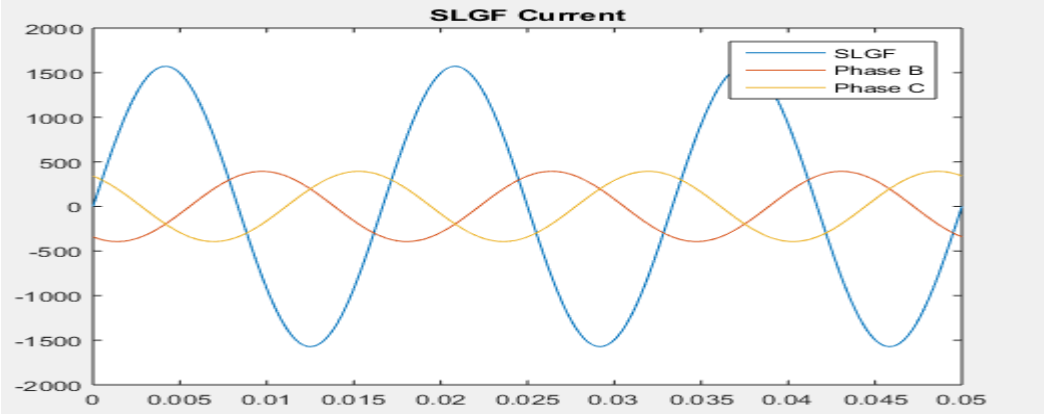

Figure 6: A graph of current vs time under single-line-to-ground fault

The value of the fault current showed the presence of the positive, negative, and zero sequence impedances. The sharp rise in the faulted phase current is consistent with the theoretical SLG fault current expression. Since:

$$\boldsymbol{Z_1 + Z_2 + Z_0} \ll \text{normal load impedance}$$

the resulting $\boldsymbol{I_f}$ becomes very large, which is clearly reflected in the waveform. This result was consistent with the theoretical result (Emechebe, 2021). The other two healthy phases maintained a peaked rated current value of 393.66A, while the faulted phase had a maximum current value of 1603A. The system interpreted the fault as single-line-to-ground fault by evaluating the sequence impedance conditions: $\boldsymbol{Z_0 \neq 0, Z_1 \approx Z_2, Z_0 \gg Z_1}$

The system threshold remained defined as:

$$\boldsymbol{I}_{\text{fault}} = \mathbf{1.1} \times \boldsymbol{I}_{\text{rated}} \quad (22)$$

From the graph, the RMS value of the faulted phase current significantly exceeds this threshold:

$$\boldsymbol{I}_{\text{RMS,SLG}} \gg \mathbf{1.1}\, \boldsymbol{I}_{\text{rated}}$$

The sharp reduction in the value of impedance and the presence of zero sequence impedance indicated the presence of single-line-to-ground fault.

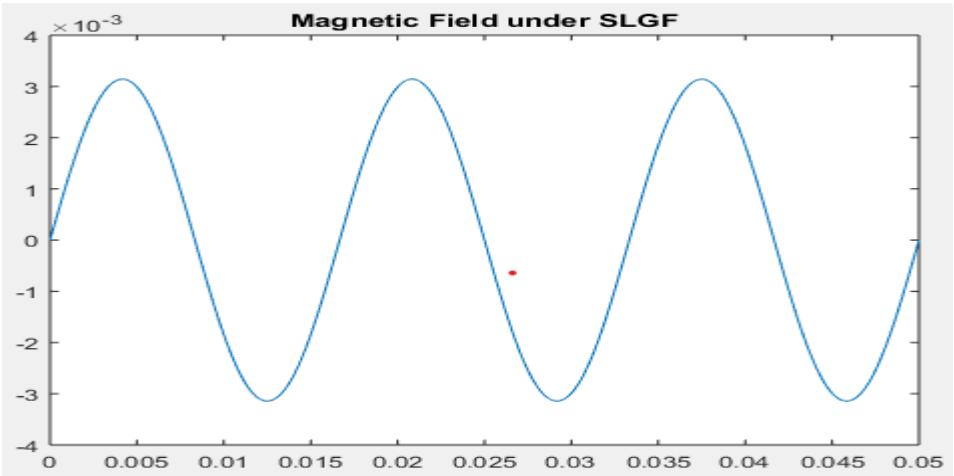

Figure 7: Magnetic field under single-line-to-ground fault

The graph above was obtained for the magnetic field under Single Line to Ground Fault. The magnetic field on the two healthy phases was not detected as abnormal. The systems responded in millisecond as shown on the vertical axis of the graph. The magnetic field under this fault was given as: (Shrawane & Sidhu, 2021; Alqusayer & Habibaballah, 2022).

$$B_{\text{fault}} = \frac{\mu_0}{2\pi r}(1.1\, I_{\text{rated}}) \quad (23)$$

$$\text{Fault Condition} = \begin{cases} 0, & B_{\text{RMS}} \leq B_{\text{fault}} \\ 1, & B_{\text{RMS}} > B_{\text{fault}} \end{cases} \quad (24)$$

Magnetic Field Strength was measured under Single Line to Ground Fault at a distance of 5.18m. The result obtained is as shown graphically. The maximum value obtained was $3.18\ x\ 10\text{^} - 3T$.

Received: 11-07-2026 / Accepted: 12-12-2025 / Published: 29-01-2026

https://doi.org/10.70118/ujet.2026.0301.10

3.3 Double Line Fault

When double line to ground fault occurred, the result showed a normal phase and two faulted phases of equal magnitude but opposite direction.

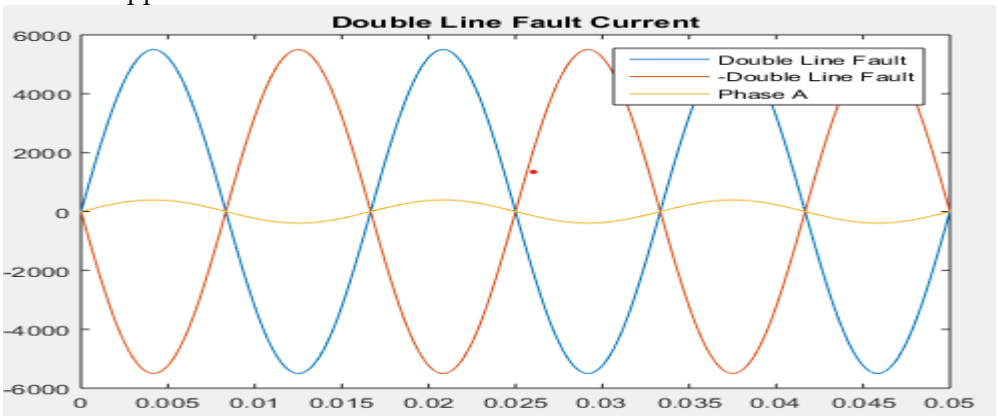

Figure 8: Fault current under double line fault

The result showed that the peak fault current was over 5500A. One line was healthy. The two faulted phases were of opposite polarity to each other. This result was consistent with the known fault current value (Emechebe, 2021). The procedure for determining the occurrence of fault under double line to ground fault was the same as in the two previous cases.

The system responded to these conditions: $|\boldsymbol{I_a}| \approx |\boldsymbol{I_b}| \gg |\boldsymbol{I_c}|$ (or any phase pair), and $\boldsymbol{Z0 \approx 0, Z1 \neq 0, Z2 \neq 0}$

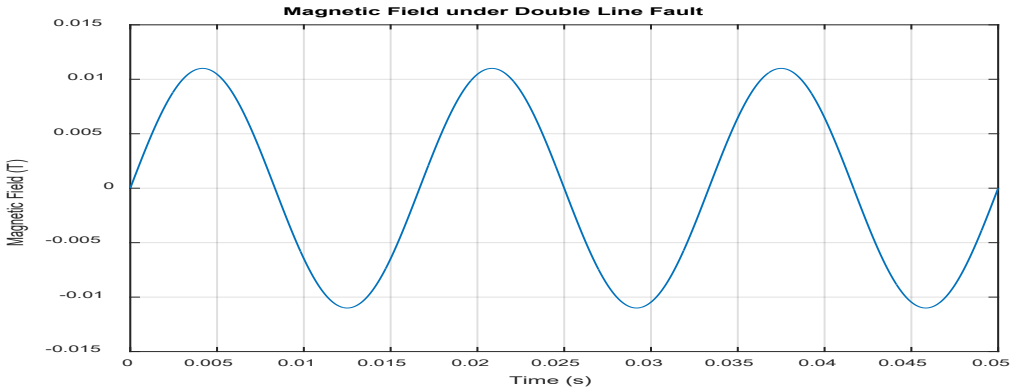

Figure 9: Magnetic field under double line fault

The magnetic field under this fault type was very high. The system followed the same procedure but used different parameters for detecting this fault type.

3.4 Fault Distance Detection

The proposed system responded to fault location, and the result was as shown in the graph below:

Received: 11-07-2026 / Accepted: 12-12-2025 / Published: 29-01-2026
https://doi.org/10.70118/ujet.2026.0301.10

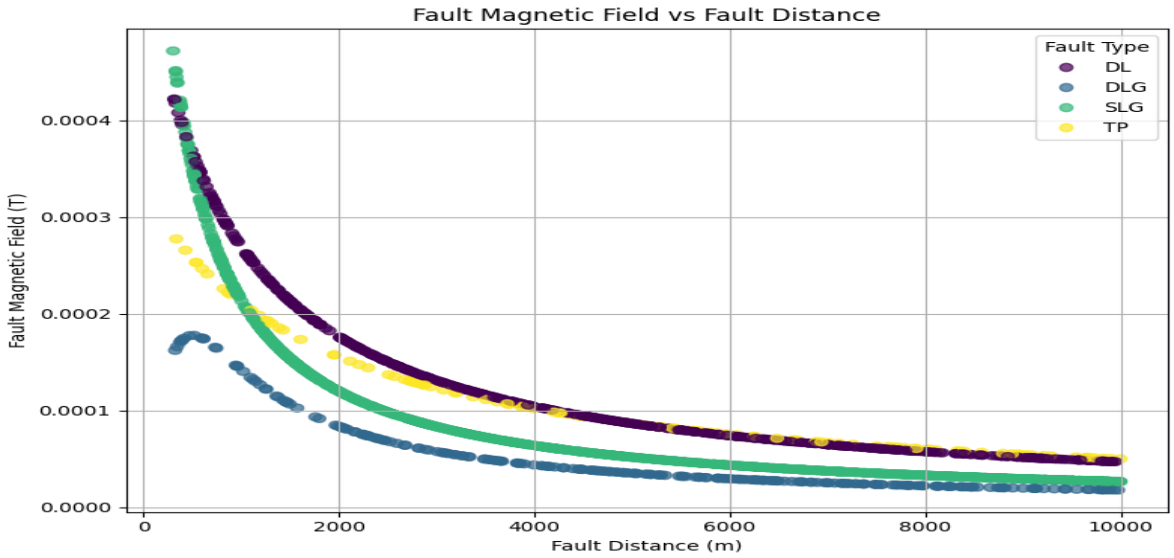

Figure 10: Magnetic field vs distance under faults

The plot shows that for all fault types, the magnetic field magnitude $\boldsymbol{B}$decreases non-linearly with distance, approximately following an inverse-distance relationship:

$B(d) \propto \frac{I_f}{d}$.

This result is consistent with the theory of the system (Shneidman, 2025).

A few numerical data read off the graph of magnetic field versus distance during the occurrence of fault for each fault scenario were as shown below:

Table 1: Single-line-to-ground fault

Distance (m)	Magnetic Field (T)
500 m	1.7×10^{-4}
1000 m	1.3×10^{-4}
2000 m	8.0×10^{-5}
5000 m	3.5×10^{-5}
10000 m	2.0×10^{-5}

Table 2: Double-line fault

Distance (m)	Magnetic Field (T)
500 m	4.0×10^{-4}
1000 m	2.0×10^{-4}
2000 m	1.5×10^{-4}
5000 m	7.0×10^{-5}
10000 m	4.5×10^{-5}

Table 3: Double-line-to-ground fault

Distance (m)	Magnetic Field (T)
500 m	4.5×10^{-4}
1000 m	3.2×10^{-4}
2000 m	1.6×10^{-4}
5000 m	6.0×10^{-5}
10000 m	3.0×10^{-5}

Table 4: Three-phase fault

Distance (m)	Magnetic Field (T)
500 m	2.6×10^{-4}
1000 m	2.0×10^{-4}
2000 m	1.3×10^{-4}
5000 m	8.0×10^{-5}
10000 m	5.0×10^{-5}

Received: 11-07-2026 / Accepted: 12-12-2025 / Published: 29-01-2026
https://doi.org/10.70118/ujet.2026.0301.10

The result obtained was sampled through 20 epochs.

3.4.1 Accuracy and validation

The result obtained showed an accuracy which was a little above 95%.
The following graph illustrates the result accuracy:

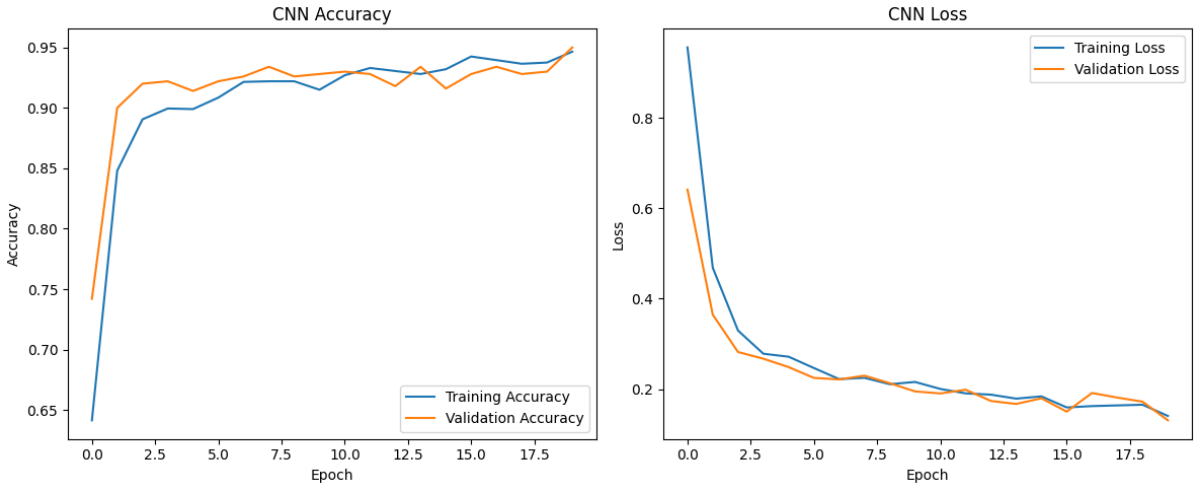

Figure 11: Result accuracy

The results showed that there was greater accuracy with an increase in epoch. The overall accuracy was 95.02%. CNN Loss showed that the loss decreased with an increase in epoch.

4.0 Conclusion

Conventional fault detection methods on the distribution system require substantial efforts in locating faults and rely on direct electrical contact with the system. Magneto-resistive sensing has proven to be different. This fault detection system is safe because it does not make contact with the distribution network. Since electric current has a corresponding magnetic field, this method detects fault current as a magnetic field and compares its magnitude with the set threshold value. During faults, current is always very high due to a substantial reduction in the impedance of the system. Thus, the magnetic field, which is proportional to the fault current, also increases beyond the threshold value. The automatic fault location feature saves significant effort and time in fault detection. Magneto-resistive sensors have high sensitivity and can detect low-level fault currents. So, it is more accurate than the conventional systems. The power requirement and cost of magneto-resistive sensors are also low compared to other fault detection systems. This fault detection and location system was modelled using Convolutional Neural Network. The system is capable of responding to different fault scenarios. The results showed that the proposed system can respond promptly to faults for remedial actions.

Acknowledgement

This research would not have been possible without the contributions of others. I appreciate God for his grace. I also appreciate my supervisor, Engr. Prof. Muhammad Uthman and Dr. O. S. Aliyu for their guidance. I appreciate my friend and brother, Engr. Moses Enang for his wonderful love and assistance. He is such an amazing fellow. I appreciate all the authors and resource persons whose inputs helped me.

References

Baladuraikannan, P. (2023). *Power system analysis: Short circuit studies* (Lecture notes). VEMU Institute of Technology, Andhra Pradesh, India.

Widodo, M. B. R., Penangsang, O., S., A., & Suryawati, I. (2021). "Fault location detection using impedance and impulse injection on 20 kV distribution system based on geographic information system". In Proceedings of the 4th International Conference on Software Engineering and Information Management (pp. 184–192). https://doi.org/10.1109/SmartIndustryCon61328.2024.10515561

Ngwenyama, M. K., Le Roux, P. F., & Ngoma, L. J. (2021). "Conventional method for electrical transmission system fault location detection". In *Proceedings of the 6th Asia Conference on Power* and Electrical Engineering.

Jeevan, M. (2022). "A review on power system faults and protection". *International Journal of Engineering*

Received: 11-07-2026 / Accepted: 12-12-2025 / Published: 29-01-2026
https://doi.org/10.70118/ujet.2026.0301.10

Research & Technology, 11(4), 395.
Stefanidou-Voziki, P., Sapountzoglou, N., Raison, B., & Dominguez-Garcia, J. L. (2022). "A review of fault location and classification methods in distribution grids". *Electric Power Systems Research, 209*, 108031. https://doi.org/10.1016/j.epsr.2022.108031
Majidi, M., Etezadi-Amoli, M., & Fadali, M. S. (2014). "A novel method for single and simultaneous fault location in distribution networks". *IEEE Transactions on Power Systems, 30*(6), 3368–3376. https://ieeexplore.ieee.org
Ogomaka, C., Udofia, K., & Okpura, N. (2020). "Open-circuit fault detection for 11 kV distribution network using ANFIS". International Journal of Power Systems, 5. https://www.iaras.org/iaras/journals/ijps
Bakar, A. H. A., Ali M. S., Tan, C. K., Mokhlis H., Arof, H., & Illias, H. A.. (2014). "High impedance fault location in 11 kV underground distribution systems using wavelet transforms". *International Journal of* Electrical Power & Energy Systems, 55, 723–730. https://doi.org/10.1016/j.ijepes.2013.10.003
Orlowski, R. (2006). Fault detection and location on 22 kV and 11 kV distribution feeders (Doctoral dissertation). Victoria University.
Majidi, M., & Etezadi-Amoli, M. (2017). "A new fault location technique in smart distribution networks using synchronized and nonsynchronized measurements". *IEEE Transactions on Power Delivery, 33*(3), 1358–1368.
Silos-Sanchez, A., Villafafila-Robles, R., & Lloret-Gallego, P. (2020). "Novel fault location algorithm for meshed distribution networks with DERs". *Electric Power Systems Research, 181*, 106182. https://doi.org/10.1016/j.epsr.2019.106182
Rao, O. S. (2020). "Magnetic field around a current-carrying conductor". *IOSR Journal of Applied Physics,* 12, 46–49.
Loete, F. (2023). "A new insight on the "S"-shape pattern of soft faults in time-domain reflectometry". Group of Electrical Engineering Paris, 24(23).
Albert, D., et al. (2022). "Power transformer hysteresis measurement". In *Proceedings of the 17th* Symposium Energieinnovation (pp. 1–11).
Mohamed, R. A. M., Gabrielli, C., Selker, J. S., Selker, F., Brooks, S. C., Ahmed, T., & Carroll, K. C.. (2021). "Comparison of fibre-optic distributed temperature sensing and high-sensitivity sensor spatial surveying of stream temperature". *Journal of Hydrology, 603*.
Shneidman, V. A. (2025). *Electricity and magnetism* (Lecture notes for Phys 121, Part II). Department of Physics, New Jersey Institute of Technology, New Jersey, USA.
Shneidman, V. A. (2025). *Electricity and magnetism* (Lecture notes for Phys 121, Part II). Department of Physics, New Jersey Institute of Technology. https://web.njit.edu-vitaly/121/notes121.pdf
Rao, O. S. (2020). "Magnetic field around a current-carrying conductor". *IOSR Journal of Applied Physics, 12*(3), 46–49. https://www.iosrjournals.org
Pratiwi, U., Haddar, G. A., & Kristiawan, M. (2020). "Arduino-based mini reed switch magnetic sensor media: Implementation in physics learning to improve students' analysing ability". *Jurnal Iqra:* Kajian Ilmu Pendidikan, 5(1), 183–193.
Fernandez, G. V. (2024). Magnetic sensors: 2024 European School of Magnetism. School of Physics, Engineering and Technology, University of York. http://hyperphysics.phy- astr.gsu.edu/hbase/magnetic/Hall.html
Kazim, M., Khawaja, A. H., Zabit, U., & Huang, Q. (2020)." Fault detection and localization for overhead 11 kV distribution lines with magnetic measurements". *IEEE Transactions on* Instrumentation and Measurement, 69(5), 20228–2038.
Wang, X., et al. (2023). "Single-phase-to-ground fault location method of overhead line based on magnetic field detection and multi-criteria fusion". *International Journal of Electrical Power & Energy Systems, 145*, 108699. https://doi.org/10.1016/j.ijepes.2022.108699
Dehkordi, S. M. (2020). "Application of deep sneural networks for load forecasting". In *Proceedings of the* 7th International Conference on Logistics and Supply Chain Management. Tehran, Iran.
Emechebe, J. N. (2021). *Power system analysis* (Lecture notes). Electrical and Electronic Engineering Department, University of Abuja, Abuja.
LeCun, Y., Bengio, Y., & Hinton, G. (2015). Deep learning. *Nature, 521*(7553), 436–444. https://doi.org/10.1038/nature14539
Shrawane, P., & Sidhu, T. S. (2021). "Performance of a noninvasive magnetic sensor-based current measurement system in power systems". *Electronics, 10*(22), 2869.
Alqusayer, A. F., & Habiballah, I. O. (2022). "Overview of single-line-to-ground fault analysis". International Journal of Engineering Research & Technology, 11(10).

Received: 11-07-2026 / Accepted: 12-12-2025 / Published: 29-01-2026

https://doi.org/10.70118/ujet.2026.0301.10